PCCP

Accepted Manuscript

ROYAL SOCIETY OF CHEMISTRY

www.rsc.org/pccp

In situ transmission electron microscopy study of sintering and redispersion phenomena over size-selected metal nanoparticles: environmental effects

Farzad Behafarid[1], Sudeep Pandey[1], Rosa E. Diaz[2], Eric A. Stach[2], Beatriz Roldan Cuenya[3*]

[1]Department of Physics, University of Central Florida, Orlando, FL 32816

[2]Center of Functional Nanomaterials, Brookhaven National Laboratory, Upton, NY

[3]Department of Physics, Ruhr University Bochum, 44780 Bochum, Germany

*e-mail: Beatriz.Roldan@rub.de

TOC

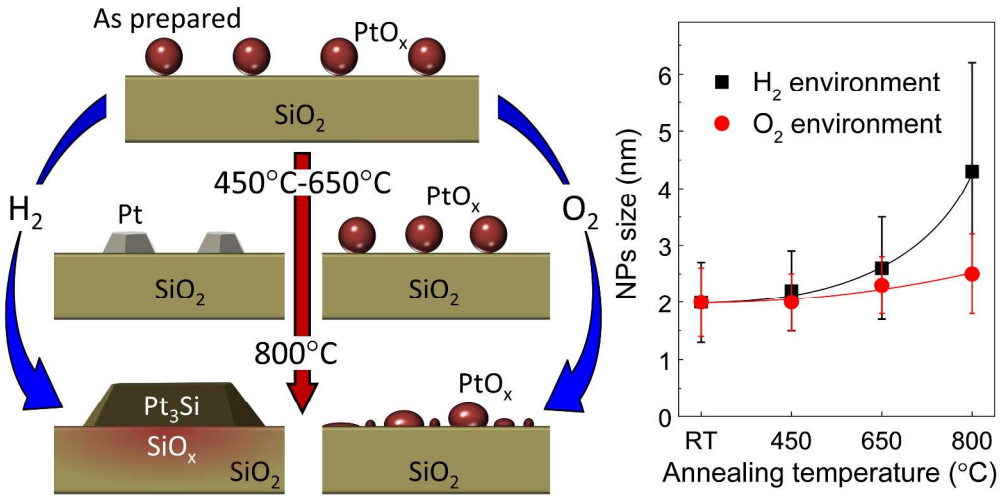

Abstract

The thermal and chemical stability of micelle-synthesized size-selected Pt nanoparticles (NPs) supported on thin SiO_2 (20 nm) films was monitored *in situ* via transmission electron microscopy (TEM) under pure hydrogen and pure oxygen environments. The coarsening treatment was performed for 30 min at each temperature (1 Torr of either O_2 or H_2), while the

TEM measurements were carried out at 1 Torr of H_2 and 0.5 Torr of O_2. Surprisingly, the NPs were found to be stable against sintering under both gaseous atmospheres up to 650°C. Nevertheless, drastic sintering via diffusion-coalescence was observed upon annealing in H_2 at 800°C. In contrast, an identically prepared sample demonstrated lack of agglomeration at the same temperature under O_2. The latter observation is ascribed to a strengthened chemical bond at the NP/support interface due to the formation of PtO_x species at low temperature. Subsequently, oxidative NP redispersion – associated with some loss of Pt due to the formation of volatile PtO_x species – is inferred from the behavior in O_2 at/above 650°C. In contrast, SiO_2 reduction catalyzed by the presence of the Pt NPs and Pt silicide formation was found in H_2 at 800°C, which might play a role in the enhanced coarsening observed. Subsequent exposure of the PtSi NPs to oxygen led to the formation of Pt/SiO_2 core/shell structures. Our findings highlight the dynamic structural transformations that nanoscale material systems experience under different environments and the important role played by their initial size, size distribution and dispersion on their stability against sintering.

Introduction

Metal nanoparticles (NPs) supported on oxides are currently used in gas sensing, optical and microelectronic devices, and catalysis applications.[1-4] Despite the intrinsic stabilizing nature of the support, sintering is observed for small NPs under certain industrial conditions, including high temperature and exposure to various chemical environments. In the field of catalysis, the decrease in the surface-to-volume ratio associated with NP agglomeration phenomena commonly leads to deactivation,[5, 6] modified selectivities, and the possible formation of unwanted byproducts.[6, 7] Since catalysts are used in roughly 90% of all commercially produced chemicals at some stage of their manufacture, understanding their stability and transformations under different environments is of the utmost importance in order to ultimately develop more durable systems.

In this study, oxide-supported Pt NPs have been selected as a model system due to their significance in catalytic processes taking place in the petroleum industry (reforming and isomerization)[8, 9], environmental remediation (removal of nitrogen oxides[10], carbon monoxide and hydrocarbons from exhaust gases), and fuel cells.[11-13] Since most of these important

reactions are carried out at high temperature (typically between 450°C and 800°C)[8-15], sintering is likely to occur.

Two main mechanisms have been proposed to explain NP sintering: (i) diffusion-coalescence (DC), where entire NPs move over the support surface and eventually collide and coalesce with other particles, and (ii) Ostwald-ripening (OR), where large NPs grow at the expense of smaller clusters via the detachment of atomic or molecular species from the smaller NPs and their diffusion over the substrate surface until they meet another NP.[5, 16, 17] It has been shown that in spite of previous claims by some groups, the shape of the NP size distribution is a not a reliable indication of the underlying coarsening mechanism.[17, 18] Some previous studies have described pronounced sintering of Pt NPs in O_2 environments (550°C to 700°C),[18-29] while others discussed greater sintering under H_2 at moderate temperatures (<400-500°C).[30-36] Furthermore, a significant increase in Pt/γ-Al_2O_3 dispersion was observed below 600°C in pure oxygen, followed by NP re-agglomeration at higher temperature.[37] For low on-stream hydrogen contents (4% H_2 in Ar), no sintering was detected on Pt/γ-Al_2O_3 up to 700°C, while the sintering rate was found to drastically increase at 600°C under low oxygen dosing (2% O_2 in Ar).[25] Other studies reported very little coarsening of Pt NPs on γ-Al_2O_3 in vacuum, N_2, H_2, or O_2 at temperatures up to 750°C, while significant agglomeration occurred in wet H_2 above 500°C.[30] For Pt NPs on SiO_2/Si(111), no sintering was observed up to 600°C in 0.5 Torr H_2 or O_2,[38] while material loss via the volatilization of PtO_x species was observed above 450°C under oxygen[38].

In order to compare sintering studies under oxidizing and reducing atmospheres from different research groups, it should be kept in mind the that coarsening phenomenona are expected to be strongly dependent on environmental conditions: not only the annealing temperature and the gas environment, but also the annealing time, composition of the gas feed (content of H_2 or O_2), pressure of gaseous environment, initial NP size and width of the NP size distribution, metal loading, initial interparticle spacing, type of metal NP/support system, as well as material characteristics (e.g. morphology, surface area, grain size and porosity) and even artifacts from the detection method used. An example of such artifacts in the case of TEM is beam induced damage that can result in local overheating of the inspected area, as well as alteration of NP-adsorbate interaction due to beam induced dissociation of gas molecules and subsequent atomic adsorption on the NP surface.

Unfortunately, the majority of the studies available are based on *ex situ* microscopic investigations,[26, 28, 30, 31, 39-41] and only a few cases display real-time data acquired under the given environments. Recently, direct observations of the sintering of physical-vapor-deposited (PVD) Pt NPs supported on γ-Al_2O_3 and SiO_2 thin films were made by Simonsen et al.[19, 22] via environmental transmission electron microscopy (E-TEM). Significant sintering was found to occur after prolonged exposure to synthetic air (21 % O_2, 79% N_2) at 650°C and a total pressure of 7.5 Torr.[19, 22] Similar work was done by Benavidez et al[42] on Pt/SiO_2, who observed no changes in the NP size distribution after 8 hours of treatment in 4.2 Torr O_2 at 550°C, although a further increase in exposure time to ten hours led to a slight increase in mean particle size. On the other hand, *in situ* extended X-ray absorption fine-structure spectroscopy (EXAFS) measurements by Matos et al.[33] demonstrated that micelle-synthesized Pt NPs supported on nanocrystalline γ-Al_2O_3 had enhanced stability after pre-treatments in pure oxygen at ~450°C (atmospheric pressure) when compared to similar exposures to hydrogen, where sintering was detected. Furthermore, samples pre-treated in O_2 at ~400°C were found to be less prone to coarsening when subsequently annealed in H_2 up to 800°C (also atmospheric pressure). In contrast, significant sintering was detected when the same sample pre-treatment was done in H_2.[33]

In this work, we utilize E-TEM to characterize the stability of homogeneously dispersed size-selected Pt NPs synthesized via inverse micelle encapsulation[4, 5, 17, 33, 38, 43] and supported on SiO_2 under pure H_2 and O_2 environments (1 Torr) up to 800°C. The role of the initial NP size, size distribution, NP/support interaction, and chemical environment in NP sintering and redispersion phenomena will be discussed.

Results and discussion

Figure 1 displays E-TEM images acquired from micelle-synthesized Pt NPs on SiO_2 (Sample S1 hereafter) after different *in situ* annealing treatments in 1 Torr hydrogen: (a) 25°C in H_2, (b) 450°C, (c) 650°C, (d) 800°C. Upon *in situ* annealing in hydrogen for 30 minutes, the average NP diameter was found to remain nearly stable from 25°C (2.0 ± 0.7 nm) to 450°C (2.2 ± 0.7 nm), while an increase in the NP size was observed at 650°C (2.6 ± 0.9 nm). Further annealing at

800°C led to drastic sintering (4.3 ± 1.9 nm). It should be noted that in parallel to the increase in the average NP diameter, a broadening of the NP size distribution was also observed, a clear indication of sintering.

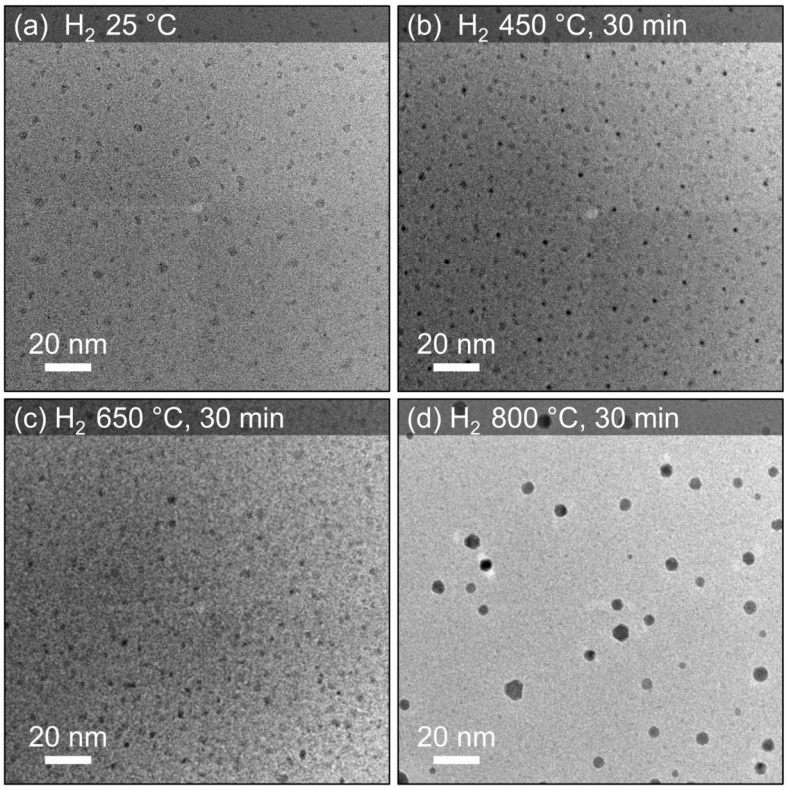

Fig. 1. *In situ* TEM images of Pt NPs supported on SiO_2 (20 nm) films (S1) acquired in a hydrogen environment (1 Torr) at the following temperatures: (a) 25°C, (b) 450°C, (c) 650°C, (d) 800°C. At each annealing step, the temperature was held constant for 30 minutes.

A second sample (S2) prepared identically to S1 was annealed under similar conditions in 1 Torr of O_2: (a) at 25°C in vacuum, (b) after 30 min at 450°C, (c) after 5 min at 650°C, (d) after 30 min at 650°C, and (e) after 30 min at 800°C, Fig. 2.

The initial average NP diameter and size distribution was found to remain nearly constant from 25°C (2.0 ± 0.6 nm) to 650°C (2.3 ± 0.7 nm). Even though similar initial NP size distributions were found for both sample S1 and S2, a drastic difference in the size distribution between both samples was observed at 800°C. Sample S2 annealed in O_2 shows an average NP diameter of 2.5 ± 0.7 nm, in clear contrast with the 4.3 ± 1.9 nm found after annealing sample S1 in H_2, highlighting the enhanced stability of the NPs against sintering in the oxidizing atmosphere. In order to further investigate this effect, sample S2 was annealed in H_2 at 450°C after the final O_2 treatment, and interestingly, an increase in the NP diameter to 3.9 ± 0.8 nm was observed, Figure 2(f).

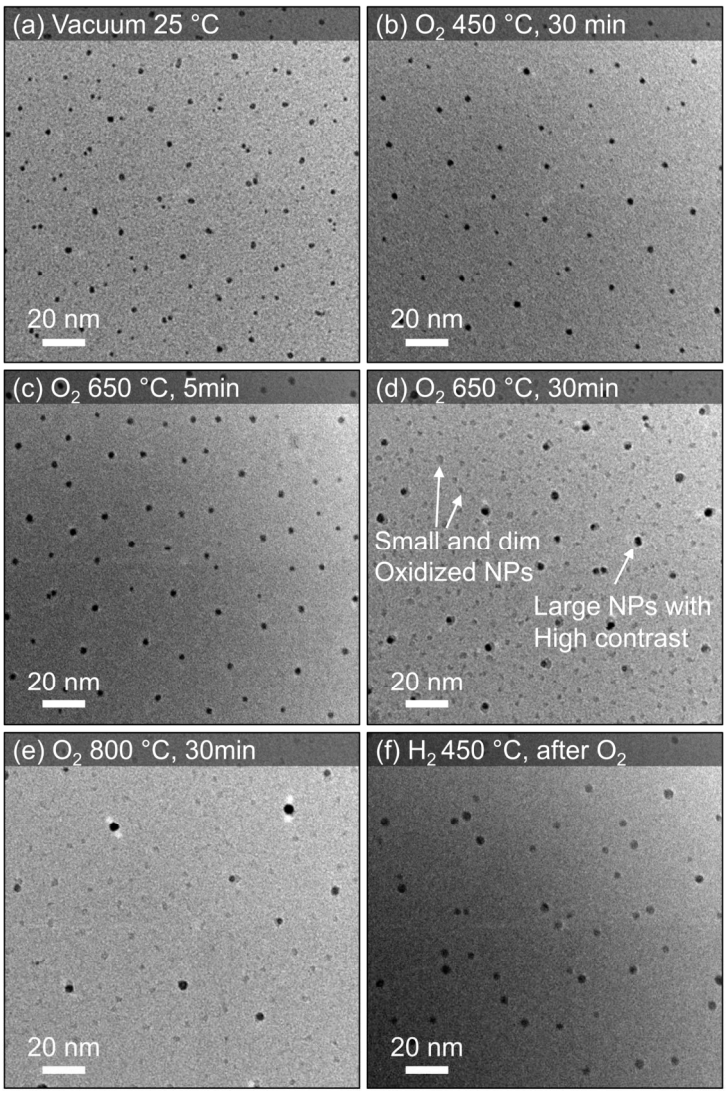

Fig. 2. *In situ* TEM images of Pt NPs supported on SiO_2 (20 nm) films (S2) acquired in an oxygen environment at the following temperatures: (a) 25°C in vacuum (as-prepared state), (b) 450°C (30 min), (c) 650°C (5 min), (d) 650°C (30 min), (e) 800°C (30 min), (f) 450°C (30 min) in 1 Torr H_2 after the O_2 treatments. The images were acquired at an O_2 pressure of 0.5 Torr after the sample was annealed at each temperature for the indicated times under 1 Torr of O_2.

The NP diameter distributions obtained from the analysis of the TEM images acquired in H_2 (a) and O_2 (b) are shown Fig. 3(a,b). Figure 3(c) displays the evolution of the average NP diameter under the different environments with increasing annealing temperature. Additional size histograms corresponding to the images in Figs. 1 and 2 are included in the supplementary information.

Our observations clearly demonstrate that Pt NPs on SiO_2 are more stable against sintering up to 800°C in an oxygen environment as compared to H_2. Recent theoretical studies on Pt/γ-Al_2O_3 have shown that hydrogen penetrates and becomes incorporated into the metal-support interface, weakening the interaction between the NPs and the support.[44, 45] The heat of adsorption of H_2 on platinum NPs is higher for Pt/SiO_2 than for Pt/γ-Al_2O_3 or Pt/TiO_2,[46] while the metal-support

interaction is larger for Pt/γ-Al_2O_3 as compared to Pt/SiO_2.[47, 48] These trends indicate that a weaker NP/support interaction exists for Pt/SiO_2 as compared to Pt/γ-Al_2O_3 in hydrogen.

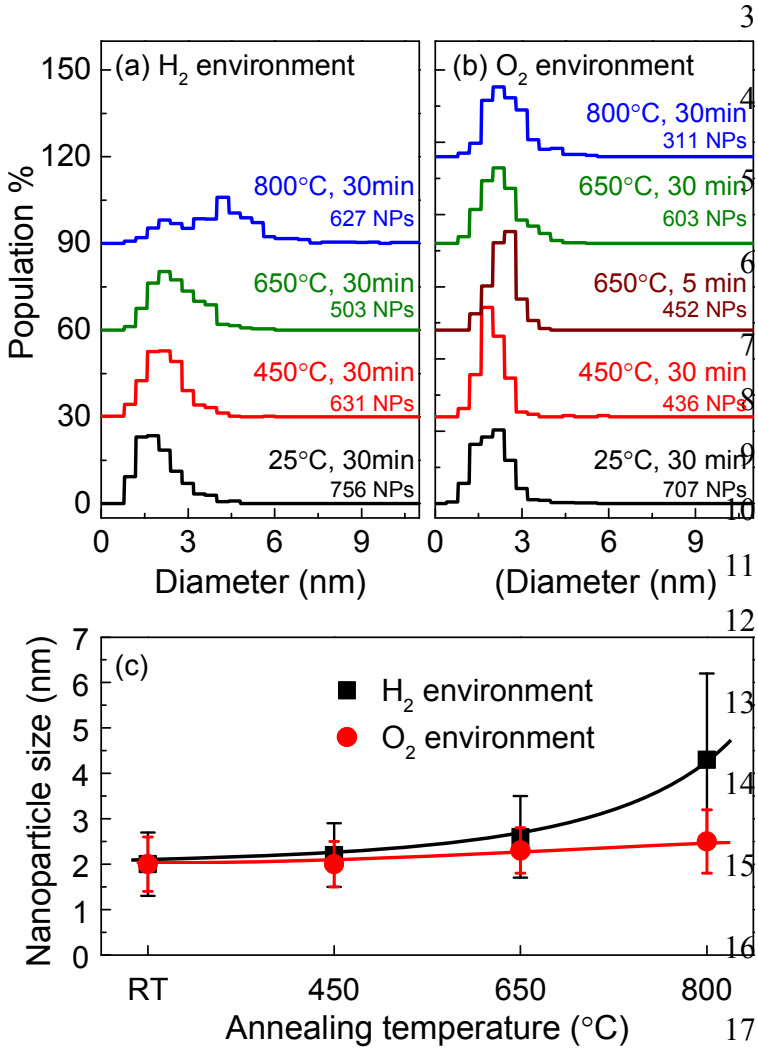

Fig. 3. Size distribution of NPs annealed *in situ* at different temperatures under (a) H_2 and (b) O_2 environments, and the resulting thermal evolution of the average NP diameter (c).

Figure 4 shows two sets of consecutive images of the Pt NPs at 650°C under H_2 (a, b, c) and O_2 (d, e, f) environments with their respective time lapse on each image. Our *in situ* TEM observations directly demonstrate the mobility of the NPs in both environments. In addition, as can be seen in Fig. 5(b), the presence of several NPs with similar size to those in the as-prepared sample surrounding a significantly larger (coarsened) Pt NP also suggests that the diffusion-coalescence process is responsible for the sintering observed under hydrogen at 800°C.

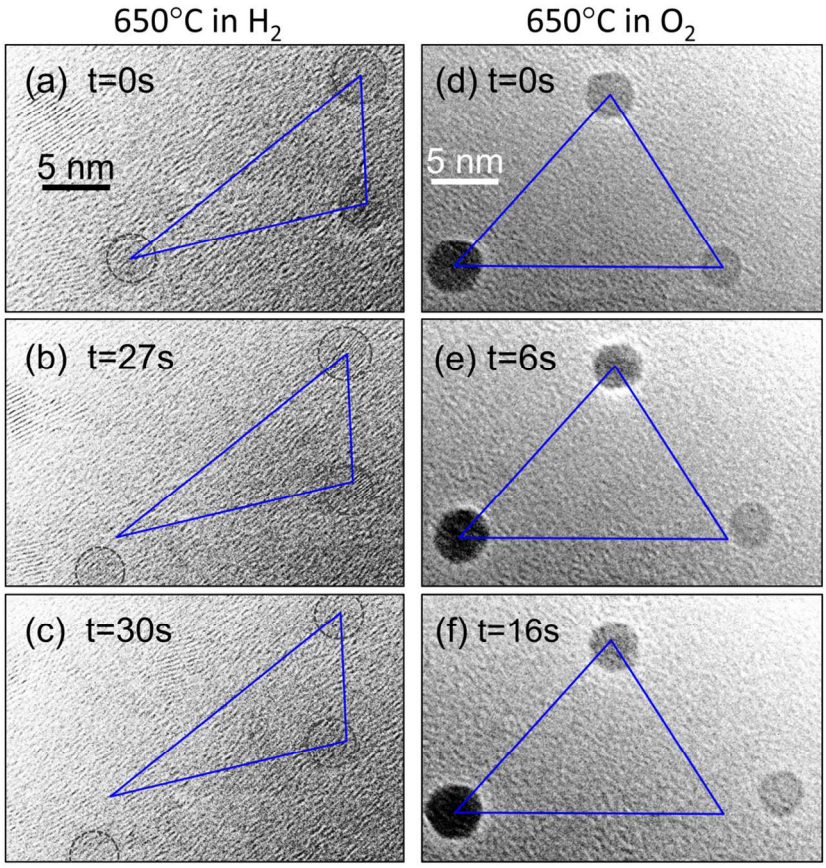

Fig. 4. TEM illustration of the mobility of entire Pt NPs in consecutive images acquired in (a, b, c) H_2 and (d, e, f) O_2 at 650°C.

Nanoparticle-support interactions have been reported to increase in O_2 environments for Pt NP/oxide support systems, leading to a decrease in NP mobility across the substrate surface.[24, 25, 32, 33] Therefore, diffusion-coalescence processes are less likely in oxygen environments,[25] as was observed here, even up to 800°C. However, although a stronger metal-support interaction would reduce the NP mobility and hinder the diffusion coalescence process, it would also reduce the energy barrier for metal-atom detachment from the NPs.[16, 17] Parker et al.[16] had derived the total energy barrier involved in the Ostwald ripening process to be $E_{tot} = \Delta H_{sub} - E^s_{ad} + H^s_m$ in which E_{tot} is equal to the metal's bulk sublimation enthalpy (ΔH_{sub}), minus the adsorption energy of a monomer on the support (E^s_{ad}), plus the diffusion barrier of a metal monomer atom on the support (H^s_m). This equation clearly shows that a higher E^s_{ad} lowers the overall OR energy barrier. In other words, a higher metal-support binding energy would make it more energetically favorable for an atom to break its bonds from the parent NP and make new bonds with the

support. Such atom-by-atom detachment could be the initial step for both NP redispersion or NP growth via OR.[49] In general, NP redispersion occurs when the detached atoms bond to trap sites on the support as either individual atoms or small clusters, while in the OR processes the detached atoms reach other NPs and contribute to their growth.[49] Variations in experimental conditions may change the most favorable trend, which might explain some of the apparent discrepancies in the literature regarding the coarsening behavior of metallic NPs in oxidizing environments. For instance, several previous studies have found that supported Pt NPs sinter significantly in O_2 at temperatures $\geq$ 600°C,[20, 23, 28, 29, 50] and oxide species[4, 37, 51] were suggested to act as intermediates in Ostwald's ripening processes. On the other hand, we have recently shown via *in situ* x-ray absorption fine-structure spectroscopy (EXAFS) and *ex situ* TEM that Pt NPs on γ-Al_2O_3 are more stable against sintering at 450°C under pure O_2 as compared to H_2.[33] The latter is in agreement with our current study as well as other reports[21, 34] showing NP growth under H_2 and NP redispersion under O_2 environments.

In addition, by comparing our present results with the related literature, it is apparent that having initially narrow NP size and interparticle distance distributions is also important. NPs synthesized using the inverse micelle encapsulation method have been shown to have a better size selection as compared to those prepared by other conventional synthesis methods such as physical vapor deposition (PVD).[17, 22, 33] NP size homogeneity, results in all particles having similar surface energies.[49] Since the difference in the NP's surface energy is the driving force for Ostwald's ripening processes, OR phenomena will be suppressed for samples with narrow NP size distributions.[17] In addition, if the interparticle distance is large, the probability of migrating species or entire NPs colliding with other particles will decrease, hence decreasing the sintering rate and favoring redispersion.[43] In fact, in previous experiments in which sintering in O_2 was observed,[19, 22] the average interparticle distances were much smaller than the ones considered here (3-5 nm vs. 18-20 nm), and the initial size distributions were also broader. Additionally, in related experiments where sintering was observed under oxidizing environments,[19, 22] longer annealing times were employed (6 h versus 30 min in our case at 650°C).

Interestingly, in our in situ study a change in the contrast of the NPs (dimmer) was observed under O_2 above 650°C in the TEM images of Fig 2 (d,e), suggesting that the dimmer NPs are flatter and likely highly oxidized. This conclusion stems from the mass-thickness contrast

mechanism prevalent in these bright-field electron micrographs; namely, for the same diameter, a lighter particle has either lighter atoms (e.g. contains more oxygen) or is thinner (e.g. flatter). A previous high pressure XPS study from our group revealed that reduced Pt NPs that are exposed to 0.5 Torr of oxygen at temperatures up to 600°C are completely oxidized and form PtO.[38] Oxidized Pt NPs have been shown to flatten as compared to metallic NPs.[52, 53] Therefore, the lack of coarsening in this study under an O_2 environment could be understood in terms of an enhanced metal-support interaction, hindering the diffusion of NPs and favoring NP redispersion. Another possibility that may play a role in the lack of sintering observed in oxygen is the elimination of a fraction of the volatile PtO_x species that are desorbed from the NPs by the microscope pumping system before re-deposition.[38] Surprisingly, an increase in the mean particle size was observed for the sample annealed in O_2 at 800°C upon subsequent exposure to 1 Torr of H_2 at 450°C. Although this sample had an average NP size similar to that of the as prepared sample, the coarsening observed upon low-temperature H_2 exposure opposes the lack of coarsening displayed by the as-prepared sample after a similar treatment. This observation may be understood in terms of NP redispersion during the treatment in oxygen resulting in small and flat clusters or isolated ions (likely oxidized) in between the NPs, which have a very weak contrast and therefore are hardly visible in the TEM images. Upon subsequent annealing in a reducing environment, such small islands would be quickly reduced and become mobile, resulting in the NP growth observed here.

High-resolution images of NPs in H_2 at 800°C (a-c) and after cooling down to 25°C and exposure to O_2 (d) are shown in Fig. 5. The crystalline structure of these NPs was determined based on their shape and the d-spacing measured from the observed lattice fringes. Remarkably, the lattice fringes observed in (a,b) are not consistent with metallic fcc Pt. The large NP shown in Fig. 5(a) has a square shape consistent with a faceted NP, seen from the [100] direction. However, the lattice spacing is almost twice that expected for d_{200} in metallic Pt (d_{100} is forbidden in the fcc structure). Similarly, the NP shown in Fig. 5(b) has a mirror symmetry consistent with a NP shown in [110] direction, and again the lattice distance is twice that of d_{220} in metallic Pt. This observation suggests that the restriction on forbidden {h,k,l} planes in an fcc lattice has been lifted. In addition, the fringes in a square metallic Pt NP are expected to run in a diagonal direction (45° rotated as compared to the edges of the NP)[45] while here the fringes run parallel to the NP edges, Fig. 5(a). These observations are consistent with the formation of Pt

silicide with a cubic Pt_3Si structure ($L1_2$ with a lattice parameter of 3.9 Å).[34, 45, 54, 55] For Pt/SiO_2 systems, such silicide formation has been reported to occur under hydrogen environment at/above 600°C [34, 45, 54, 55] but not in vacuum, even after treatments up to 800°C.[56] This phenomenon reflects the catalytic reduction of SiO_2 in H_2 mediated by the presence of the Pt NPs.[47, 57-59] The reduction of the ultrathin SiO_2 membrane (20 nm) under our experimental conditions is also evident in Fig. 5(c), in which the round feature has a d-spacing of 3.1 Å, which is consistent with silicon (111).[57, 58] Such reduction of the SiO_2 support in our sample most likely occurred under a Pt NP, which has subsequently disappeared due to coarsening, exposing the NP/support interface. Interestingly, a different type of fringe could be seen in the lower and upper edges of the square NP in Fig. 5a. Since the NP thickness decreases at the side facets, this may allow the Si substrate features to become dominant. These lattice fringes (d-spacing of 3.1 Å) match those of Si(111), confirming that the substrate is reduced underneath the NP.

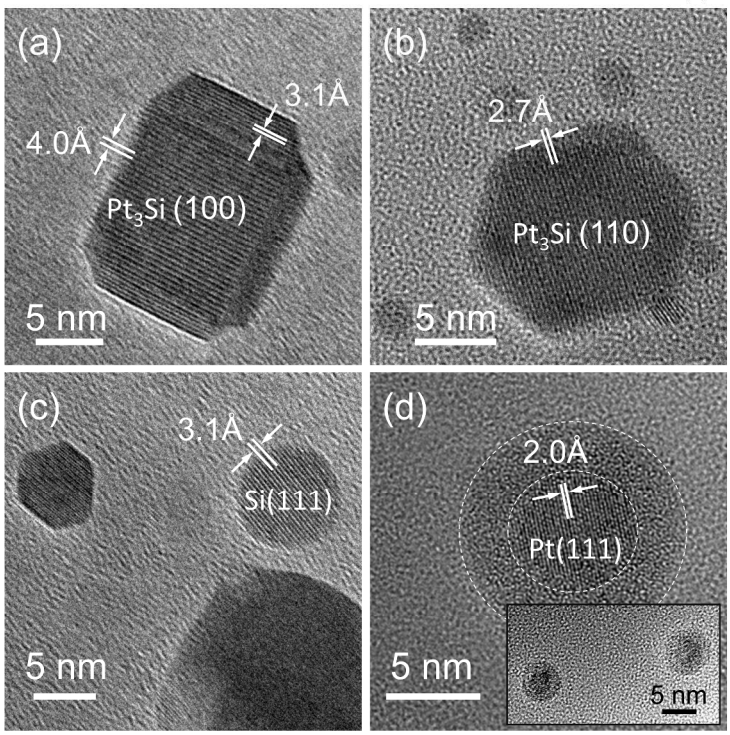

Fig. 5. High resolution TEM images of Pt NPs acquired at 800°C in H_2 (a-c) and of NPs in the same sample measured after cooling to 25°C and subsequent exposure to O_2 (d).

Figure 5(d) shows the sample that was annealed in H_2 at 800°C after it was cooled to 25°C and was exposed to O_2. The NPs show now a core-shell structure with a crystalline core and an amorphous shell. The 2.0 Å lattice spacing of the core matches the metallic structure of Pt (d_{200}). These data evidence that O_2 exposure results in the outward segregation of Si from Pt silicide

due its higher oxygen affinity and the formation of a SiO_x shell, leaving the NP core as pure Pt.[59] However, the possible presence of Pt oxide species in the NP shell cannot be completely ruled out. The inset in Fig. 5(d) shows additional examples of the observed core-shell structures.

Figure 6 schematically summarizes our observations for both samples. The as-prepared samples are initially oxidized and have a narrow size distribution (a). Annealing in a hydrogen environment in the temperature range of 450°C-650°C results in the reduction of the NPs to metallic Pt followed by faceting, with only moderate mobility and limited coarsening (b). Increasing the temperature to 800°C in H_2 results in catalytic SiO_2 reduction due to the presence of the Pt NPs, Pt silicide formation, and severe NP sintering, (c). Lastly, cooling the sample to room temperature and exposing it to O_2 results in the formation of core-shell structures, (d).

In clear contrast, annealing the analogous as-prepared sample in O_2 at 450°C-650°C has no significant effect on the NP average size, Fig. 2(e). Although moderate mobility is expected, the large interparticle distance in our sample hinders the diffusion/coalescence in the time scale of this study. However, annealing at high temperature led to the disruption of the NPs and their redispersion, resulting in the formation of small Pt oxide clusters in between the larger NPs, Fig. 2(f). A final annealing of the sample at 450°C in H_2 after cooling the sample to room temperature resulted in the reduction of the PtO_x clusters and their consequent agglomeration with Pt NPs, which is observed as an overall coarsening effect.

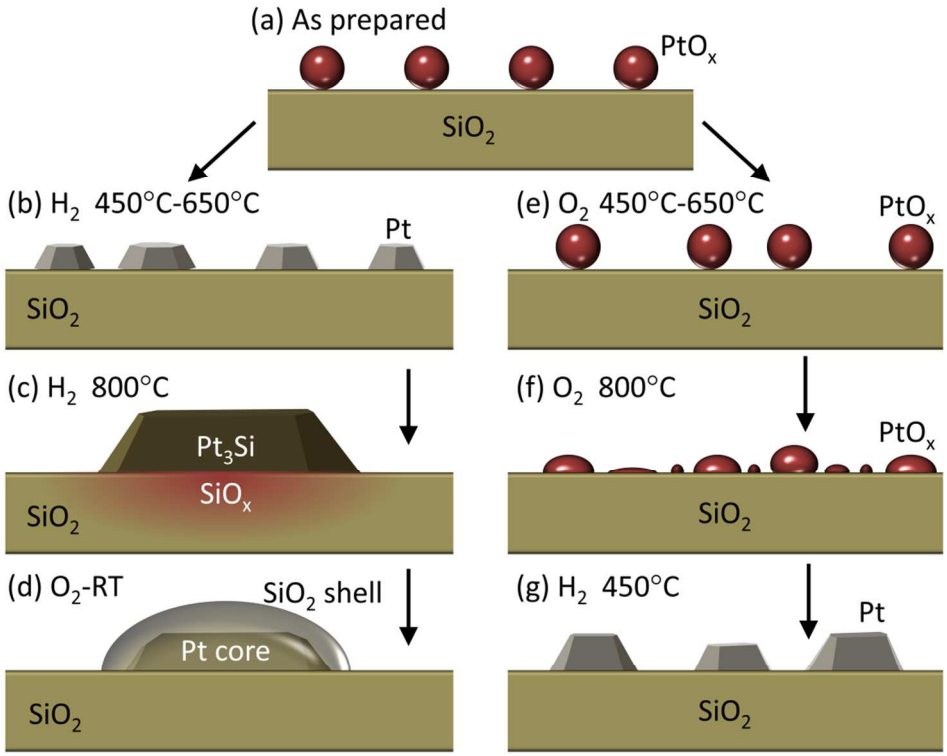

Fig. 6. Schematic cartoon depicting environmental effects on NP morphology and mobility. (a) Oxidized as prepared sample, (b) reduction of the NPs under H_2 at 450°C-650°C and moderate NP mobility. (c) Annealing at high temperature (800°C) under H_2 results in catalytic reduction of SiO_2, Pt-Si alloy formation, and severe coarsening. (d) Exposure of the sample coarsened in H_2 to O_2 results in the formation of core-shell structures. (e) In contrast, heat treatment in O_2 (450°C-650°C) only results in moderate mobility. (f) High temperature annealing in O_2 results in NP disruption and redispertion as well as NP flattening. (g) At last, annealing the sample previously treated in O_2, under a H_2 environment results in coarsening due to the reduction and agglomeration of small Pt oxide clusters dispersed between the original NPs.

Conclusion

Our *in situ* TEM study of the stability of micelle-synthesized Pt NPs revealed drastic changes in the sample morphology with increasing temperature in hydrogen, with marked sintering via diffusion-coalescence starting at 650°C and being most prominent at 800°C, where the formation of large faceted NPs was observed. The reduction of the SiO_2 support and the formation of Pt

silicide were demonstrated based on HRTEM images. Exposing the platinum silicide to O_2 at room temperature resulted in the outward diffusion of Si and formation of a silicon oxide shell and a metallic Pt core. In contrast, no sintering was observed when an identical sample was annealed in pure oxygen under the same conditions, i.e. up to 800°C. To the best of our knowledge, this is the only experimental study that shows enhanced stability of small Pt NPs against coarsening up to 800°C in O_2. Some groups have reported significant coarsening under O_2 (550°C to 700°C).[18-29, 39] Others have shown minimal sintering in O_2,[30-36] but at much lower temperatures (<550°C). Such enhanced stability is assigned to the strengthening of the Pt NP/SiO_2 interface upon PtO_x formation and to NP redispersion. This is in agreement with the observed change in the NP contrast (dimmer NPs) indicative of flatter NPs. The NP redispersion was also confirmed by the subsequent low temperature coarsening (450°C) observed for this sample in H_2 due to the reduction of small ions/PtO_x clusters distributed between the larger NPs and their contribution to NP growth. Although silicon oxide has been traditionally considered as a "non-reducible" support, here we provide direct experimental evidence for the role of Pt NPs in the catalytic reduction of SiO_2 to Si under much lower temperatures than those required in the absence of the NPs. Also, it was found that the Pt NP/SiO_2 system could form a core-shell structure resulting in Pt silicide formation upon annealing in H_2 and the subsequent formation of a SiO_2 shell upon exposure to O_2. Cyclic treatments in oxidizing and reducing environments are a common practice in the catalysis industry, and for the case of Pt NP/SiO_2, such treatments could result in the encapsulation of the Pt NPs by a SiO_x layer.

Experimental

The technique of inverse micelle encapsulation[4, 60] was employed to prepare the samples presented here. A polystyrene-2vinylpiridine [PS(16000)-P2VP(3500)] diblock copolymer was dissolved in toluene to create inverse micelles, and the micellar cages were loaded with a H_2PtCl_6 platinum precursor with 0.1 metal-to-P2VP ratio. The samples were then drop coated onto SiO_2(20 nm)/Si TEM grids (SO100-A20Q33). Two samples were prepared using the same NP solution. Subsequently, the samples underwent an O_2 plasma treatment in ultrahigh vacuum (UHV) for the removal of the polymeric ligands (P_{O2} =4×10^{-5} mbar, 120 min). X-ray photoelectron spectroscopy (XPS) measurements confirmed the absence of chlorine and carbon

contaminations after the plasma treatment. The as-prepared Pt NPs were found to be oxidized due to the O_2-plasma treatment.[4] Since the samples were transferred in air to Brookhaven National Laboratory (BNL) for the E-TEM work, a 5 min O_2-plasma treatment was done at BNL before the microscopy measurements in order to ensure the complete removal of adventitious carbon from the NP surface.

In situ TEM analysis was done using an aberration-corrected 300 keV transmission electron microscope (FEI Titan 80-300) equipped with a differentially pumped environmental cell and a post-specimen CEOS aberration-corrector. Image acquisition used both a Gatan Orius camera and a Gatan Ultrascan camera. Two identically-prepared but separate samples were used for the H_2 and O_2 treatments. In our experiments, the pressure was maintained at 1 Torr at all temperatures during the treatments in hydrogen (sample S1) and oxygen (S2), but reduced to 0.5 Torr for the acquisition of the images in oxygen. In both environments, the investigated sample temperatures were: 25°C (room temperature), 450°C, 650°C, and 800°C. The samples were kept for 30 min at each temperature. The sample temperature was measured with a thermocouple attached to a furnace in the vicinity of the sample and may have a ±10°C error as compared to the actual temperature on the TEM grid. For the 650°C treatment in O_2, two datasets were acquired, a first one after a 5-minute exposure, and a second one after 30 minutes. After the treatment of S2 in oxygen at 800°C, the sample was subsequently reduced in H_2 at 450°C while sample S1 treated at 800°C in H_2, was cooled to room temperature (25°C), and was exposed to O_2.

Beam-damage effects were carefully monitored. The beam density varies between different images depending on the magnification, with higher density for higher magnification. A typical dose of 800 electrons/Å^2 for a magnification of 530kx and a value of 400 electrons/Å^2 for a magnification of 130kx were used. The exposure time was varied in the order of 0.1-1 seconds. Drastic changes were observed in our sample morphology under combined O_2 and e-beam irradiation, in particular, the formation of shell-like crystalline structures around the NPs suggestive of significant oxidation due to e-beam-induced O_2 dissociation. Such structures were found to grow into whiskers with increasing e-beam exposure time (not shown). Such effects were not observed under identical dosing conditions in hydrogen. Therefore, in order to minimize undesired measurement artifacts, which might obscure the real O_2-mediated sintering

phenomena, i.e., those occurring in the absence of the electron beam, images in O_2 were acquired immediately after reaching a given temperature. The beam was then turned off, and then the sample was kept at the given temperature for 30 min, when the beam was turned back on to check the final state of the sample.

Acknowledgement

Financial support from the U.S. Department of Energy (DE-FG02-08ER15995) is greatly appreciated. Use of the electron microscopy facilities at the Center for Functional Nanomaterials, Brookhaven National Laboratory, which is supported by the U.S. Department of Energy, Office of Basic Energy Sciences, under contract DE-AC02-98CH10886 is acknowledged. This work was also partially funded by the Cluster of Excellence Ruhr Explores Solvation (RESOLV) (EXC 1069) funded by the Deutsche Forschungsgemeinschaft.

References

1. Zhang, L.; Gu, F. X.; Chan, J. M.; Wang, A. Z.; Langer, R. S.; Farokhzad, O. C. Nanoparticles in Medicine: Therapeutic Applications and Developments. *Clin. Pharmacol .Ther.* **2007,** 83, 761-769.

2. Chen, Z.; Taflove, A.; Backman, V. Photonic nanojet enhancement of backscattering of light by nanoparticles: a potential novel visible-light ultramicroscopy technique. *Opt. Express* **2004,** 12, 1214.

3. Chow, L.; Lupan, O.; Chai, G.; Khallaf, H.; Ono, L. K.; Roldan Cuenya, B.; Tiginyanu, I. M.; Ursaki, V. V.; Sontea, V.; Schulte, A. Synthesis and characterization of Cu-doped ZnO one-dimensional structures for miniaturized sensor applications with faster response. *Sensor Actuat. A-Phys.* **2013,** 189, 399-408.

4. Ono, L. K.; Croy, J. R.; Heinrich, H.; Roldan Cuenya, B. Oxygen Chemisorption, Formation, and Thermal Stability of Pt Oxides on Pt Nanoparticles Supported on SiO_2/Si(001): Size Effects. *J. Phys. Chem. C* **2011,** 115, 16856-16866.

5. Behafarid, F.; Roldan Cuenya, B. Towards the Understanding of Sintering Phenomena at the Nanoscale: Geometric and Environmental Effects. *Top. Catal.* **2013,** 56, 1542-1559.

6. Bartholomew, C. H. Mechanisms of catalyst deactivation. *Appl. Catal. A-Gen.* **2001,** 212, 17-60.

7. Haruta, M. Size- and support-dependency in the catalysis of gold. *Catal. Today* **1997,** 36, 153-166.

8. Guyot-Sionnest, N. S.; Villain, F.; Bazin, D.; Dexpert, H.; Peltier, F.; Lynch, J.; Bournonville, J. P. In situ high temperature and high pressure exafs studie of Pt/Al_2O_3 catalysts. Part I: Reduction and deactivation. *Catal. Lett.* **1991,** 8, 283-295.

9. Hamoule, T.; Peyrovi, M. H.; Rashidzadeh, M.; Toosi, M. R. Catalytic reforming of n-Heptane over Pt/Al-HMS catalysts. *Catal. Commun.* **2011,** 16, 234-239.

10. Weiss, B. M.; Iglesia, E. NO Oxidation Catalysis on Pt Clusters: Elementary Steps, Structural Requirements, and Synergistic Effects of NO_2 Adsorption Sites. *J. Phys.Chem.C* **2009,** 113, 13331-13340.

11. Bell, A. T. The impact of nanoscience on heterogeneous catalysis. *Science* **2003,** 299, 1688-1691.

12. Li, Y. M.; Somorjai, G. A. Nanoscale Advances in Catalysis and Energy Applications. *Nano Letters* **2010,** 10, 2289-2295.

13. de Souza, S. Thin-film solid oxide fuel cell with high performance at low-temperature. *Solid State Ionics* **1997,** 98, 57-61.

14. Oh, Y. A highly active catalyst, Ni/Ce–ZrO_2/θ-Al_2O_3, for on-site H_2 generation by steam methane reforming: pretreatment effect. *Int. J. Hydorgen. Energ.* **2003,** 28, 1387-1392.

15. Rashkeev, S. N.; Ginosar, D. M.; Petkovic, L. M.; Farrell, H. H. Catalytic activity of supported metal particles for sulfuric acid decomposition reaction. *Catal. Today* **2009,** 139, 291-298.

16. Parker, S.; Campbell, C. Kinetic model for sintering of supported metal particles with improved size-dependent energetics and applications to Au on TiO_2(110). *Phys. Rev. B* **2007,** 75.

17. Behafarid, F.; Roldan Cuenya, B. Coarsening phenomena of metal nanoparticles and the influence of the support pre-treatment: Pt/TiO_2(110). *Surf. Sci.* **2012,** 606, 908-918.

18. Datye, A. K.; Xu, Q.; Kharas, K. C.; McCarty, J. M. Particle size distributions in heterogeneous catalysts: What do they tell us about the sintering mechanism? *Catal. Today* **2006,** 111, 59-67.

19. Simonsen, S. B.; Chorkendorff, I.; Dahl, S.; Skoglundh, M.; Sehested, J.; Helveg, S. Direct Observations of Oxygen-induced Platinum Nanoparticle Ripening Studied by In Situ TEM. *J. Am. Chem. Soc* **2010,** 132, 7968-7975.

20. Baker, R. Continuous observation of the particle size behavior of platinum on alumina. *J. Catal.* **1975,** 38, 510-513.

21. Monzón, A.; Garetto, T. F.; Borgna, A. Sintering and redispersion of Pt/γ-Al_2O_3 catalysts: a kinetic model. *Appl. Catal. L. A-Gen* **2003,** 248, 279-289.

22. Simonsen, S. B.; Chorkendorff, I.; Dahl, S.; Skoglundh, M.; Sehested, J.; Helveg, S. Ostwald ripening in a Pt/SiO_2 model catalyst studied by in situ TEM. *J. Catal.* **2011,** 281, 147-155.

23. White, D. Electron microscope studies of platinum/alumina reforming catalysts. *J. Catal.* **1983,** 81, 119-130.

24. Fiedorow, R. The sintering of supported metal catalysts II. Comparison of sintering rates of supported Pt, Ir, and Rh catalysts in hydrogen and oxygen. *J. Catal.* **1978,** 51, 193-202.

25. Loof, P. Rapid Sintering in NO of Nanometer-Sized Pt Particles on γ-Al_2O_3 Observed by CO Temperature-Programmed Desorption and Transmission Electron Microscopy. *J. Catal.* **1993,** 144, 60-76.

26. Smith, D. The characterisation of a model platinum/alumina catalyst by high-resolution electron microscopy. *J. Catal.* **1983,** 81, 107-118.

27. Nagai, Y.; Dohmae, K.; Ikeda, Y.; Takagi, N.; Hara, N.; Tanabe, T.; Guilera, G.; Pascarelli, S.; Newton, M. A.; Takahashi, N.; Shinjoh, H.; Matsumoto, S. i. In situ observation of

platinum sintering on ceria-based oxide for autoexhaust catalysts using Turbo-XAS. *Catal. Today* **2011,** 175, 133-140.

28. Yang, J.; Tschamber, V.; Habermacher, D.; Garin, F.; Gilot, P. Effect of sintering on the catalytic activity of a Pt based catalyst for CO oxidation: Experiments and modeling. *Appl. Catal. B-Environ.* **2008,** 83, 229-239.

29. Auvray, X.; Pingel, T.; Olsson, E.; Olsson, L. The effect gas composition during thermal aging on the dispersion and NO oxidation activity over Pt/Al_2O_3 catalysts. *Appl. Catal. B-Environ.* **2013,** 129, 517-527.

30. Chu, Y. On the sintering of platinum on alumina model catalyst. *J. Catal.* **1978,** 55, 281-298.

31. Glassl, H. Electron microscopy of Pt/Al_2O_3 model catalysts II. Sintering in atmospheres of H_2, O_2 and Ar. *J. Catal.* **1981,** 68, 388-396.

32. Hassan, S. The effect of different atmospheres on the sintering of Pt/Al_2O_3 reforming catalysts. *J. Catal.* **1976,** 44, 5-14.

33. Matos, J.; Ono, L. K.; Behafarid, F.; Croy, J. R.; Mostafa, S.; DeLaRiva, A. T.; Datye, A. K.; Frenkel, A. I.; Roldan Cuenya, B. In situ coarsening study of inverse micelle-prepared Pt nanoparticles supported on γ-Al_2O_3: pretreatment and environmental effects. *Phys. Chem. Chem. Phys.* **2012,** 14, 11457.

34. Lamber, R.; Romanowski, W. Dispersion changes of platinum supported on silica glass during thermal treatment in oxygen and hydrogen atmospheres. *J. Catal.* **1987,** 105, 213-226.

35. Sellin, R. m.; Grolleau, C. d.; Arrii-Clacens, S.; Pronier, S. p.; Clacens, J.-M.; Coutanceau, C.; Léger, J.-M. Effects of Temperature and Atmosphere on Carbon-Supported Platinum Fuel Cell Catalysts. *J. Phys. Chem. C* **2009,** 113, 21735-21744.

36. Bournonville, J. P.; Martino, G. Sintering of Alumina Supported Platinum. *Stud. Surf. Sci. Catal.* **1980,** 6, 159-166.

37. Fiedorow, R.; Wanke, S. The sintering of supported metal catalystsI. Redispersion of supported platinum in oxygen. *J. Catal.* **1976,** 43, 34-42.

38. Porsgaard, S.; Merte, L. R.; Ono, L. K.; Behafarid, F.; Matos, J.; Helveg, S.; Salmeron, M.; Roldan Cuenya, B.; Besenbacher, F. Stability of Platinum Nanoparticles Supported on SiO_2/Si(111): A High-Pressure X-ray Photoelectron Spectroscopy Study. *ACS Nano* **2012**, 121120155741008.

39. Nazarpoor, Z.; Ma, S.; Fanson, P. T.; Alexeev, O. S.; Amiridis, M. D. O_2 plasma activation of dendrimer-derived Pt/γ-Al_2O_3 catalysts. *J. Catal.* **2012,** 290, 26-36.

40. Veith, G. M.; Lupini, A. R.; Rashkeev, S.; Pennycook, S. J.; Mullins, D. R.; Schwartz, V.; Bridges, C. A.; Dudney, N. J. Thermal stability and catalytic activity of gold nanoparticles supported on silica. *J. Catal.* **2009,** 262, 92-101.

41. Alexeev, O. Temperature-Programmed Desorption of Hydrogen from Platinum Particles on γ-Al_2O_3: Evidence of Platinum-Catalyzed Dehydroxylation of γ-Al_2O_3. *J. Catal.* **1999,** 185, 170-181.

42. Benavidez, A. D.; Kovarik, L.; Genc, A.; Agrawal, N.; Larsson, E. M.; Hansen, T. W.; Karim, A. M.; Datye, A. K. Environmental Transmission Electron Microscopy Study of the Origins of Anomalous Particle Size Distributions in Supported Metal Catalysts. *ACS Catal.* **2012,** 2, 2349-2356.

43. Ono, L. K.; Roldan Cuenya, B. Effect of interparticle interaction on the low temperature oxidation of CO over size-selected Au nanocatalysts supported on ultrathin TiC films. *Catal. Lett.* **2007,** 113, 86-94.

44. Mager-Maury, C.; Bonnard, G.; Chizallet, C.; Sautet, P.; Raybaud, P. H_2-Induced Reconstruction of Supported Pt Clusters: Metal-Support Interaction versus Surface Hydride. *ChemCatChem* **2011,** 3, 200-207.

45. Wang, D. Silicide formation on a Pt/SiO_2 model catalyst studied by TEM, EELS, and EDXS. *J. Catal.* **2003,** 219, 434-441.

46. Vannice, M. Direct measurements of heats of adsorption on platinum catalysts I. H_2 on Pt dispersed on SiO_2, Al_2O_3, SiO_2-Al_2O_3, and TiO_2. *J. Catal.* **1985,** 95, 57-70.

47. Arai, M.; Ishikawa, T.; Nakayama, T.; Nishiyama, Y. Effects of metal—support interaction and temperature on the sintering of Pt and Ag particles supported on inorganic solids. *J. Colloid. Interf. sci.* **1984,** 97, 254-265.

48. Lee, T. J. Redispersion of supported platinum catalysts. *J. Catal.* **1984,** 90, 279-291.

49. Ouyang, R.; Liu, J.-X.; Li, W.-X. Atomistic Theory of Ostwald Ripening and Disintegration of Supported Metal Particles under Reaction Conditions. *J. Am. Chem. Soc.* **2013**, 130125092846007.

50. Harris, P. The sintering of platinum particles in an alumina-supported catalyst: Further transmission electron microscopy studies. *J. Catal.* **1986,** 97, 527-542.

51. LÖÖf, P.; Kasemo, B.; BjÖrnkvist, L.; Andersson, S.; Frestad, A. Tpd And Xps Studies of Co and No on Highly Dispersed PT+RH Automotive Exhaust Catalysts: Evidence for Noble Metal-Ceria Interaction. *Stud. Surf. Sci. Catal.* **1991,** 71, 253-274.

52. Merte, L. R.; Ahmadi, M.; Behafarid, F.; Ono, L. K.; Lira, E.; Matos, J.; Li, L.; Yang, J. C.; Roldan Cuenya, B. Correlating Catalytic Methanol Oxidation with the Structure and Oxidation State of Size-Selected Pt Nanoparticles. *ACS Catal.* **2013,** 3, 1460-1468.

53. Markusse, A. P.; Kuster, B. F. M.; Koningsberger, D. C.; Marin, G. B. Platinum deactivation: in situ EXAFS during aqueous alcohol oxidation reaction. *Catal. Lett.* **1998,** 55, 141-145.

54. Lamber, R.; Jaeger, N. I. On the reaction of Pt with SiO_2 substrates: Observation of the Pt_3Si phase with the Cu_3Au superstructure. *J. Appl. Phys.* **1991,** 70, 457.

55. Wang, D.; Penner, S.; Su, D. S.; Rupprechter, G.; Hayek, K.; Schlögl, R. SiO_2-supported Pt particles studied by electron microscopy. *Mater. Chem. Phys.* **2003,** 81, 341-344.

56. Yu, R.; Song, H.; Zhang, X. F.; Yang, P. D. Thermal wetting of platinum nanocrystals on silica surface. *J. Phys. Chem. B* **2005,** 109, 6940-6943.

57. Li, H.; Huang, X. J.; Chen, L. Q.; Zhou, G. W.; Zhang, Z.; Yu, D. P.; Mo, Y. J.; Pei, N. The crystal structural evolution of nano-Si anode caused by lithium insertion and extraction at room temperature. *Solid State Ionics* **2000,** 135, 181-191.

58. Holmes, J. D.; Johnston, K. P.; Doty, R. C.; Korgel, B. A. Control of Thickness and Orientation of Solution-Grown Silicon Nanowires. *Science* **2000,** 287, 1471-1473.

59. Cros, A.; Pollak, R. A.; Tu, K. N. Room-temperature oxidation of Ni, Pd, and Pt silicides. *J. Appl. phys.* **1985,** 57, 2253.

60. Eastoe, J.; Hollamby, M. J.; Hudson, L. Recent advances in nanoparticle synthesis with reversed micelles. *Adv. Colloid. Interfac.* **2006,** 128-130, 5-15.